ce/papers Proceedings in civil engineering

Ernst & Sohn A Wiley Brand

Full paper

Ductile Fracture in WAAM-Fabricated High Strength Steel for Structural Applications

Trayana Tankova[1] | Haqar El Bamby[1] | Milan Veljkovic[1]

Correspondence

Dr. Trayana Tankova
Delft University of Technology
Department of Engineering Structures
Stevinweg I
2628CN Delft
Email: t.tankova@tudelft.nl

[1] Delft University of Technology, Delft, the Netherlands

Abstract

This study investigates the ductile fracture behaviour of coupon-like specimens produced by Wire Arc Additive Manufacturing (WAAM) using AM70 high-strength low-alloy steel wire. Experimental testing under uniaxial tension and shear loading was conducted, supported by digital image correlation to capture strain fields. The material's plastic response was calibrated using a combination of true stress-strain conversion, a weighted average model for post-necking behaviour, and finite element simulations. Ductile damage was implemented numerically to simulate fracture, showing good agreement with experimental results in both failure mode and stress-strain response. The AM70 WAAM material exhibited a fracture strain of 0.65 in uniaxial tension and 0.70 in shear, indicating enhanced ductility compared to high-strength steels and previously reported WAAM references. Despite a moderate reduction in yield strength the material showed promising mechanical performance, particularly under shear-dominated conditions. These findings suggest the suitability of AM70 WAAM components for applications requiring high deformation capacity. The validated modelling approach offers a robust basis for predicting failure, and future work will explore the application of advanced fracture models for improved accuracy across diverse loading conditions.

Keywords

Steel, Wire Arc Additive Manufacturing, Material properties, FE modelling

1 Introduction

Wire Arc Additive Manufacturing (WAAM) has emerged as an innovative technology for producing large-scale components, offering substantial benefits in reducing material waste and production time for complex geometries. However, the unique layered microstructure and inherent material characteristics of WAAM-fabricated components introduce a need for a better understanding of mechanical behaviours, particularly in ductile fracture under multiaxial stress conditions. Understanding these fracture mechanisms is crucial for optimising structural designs, yet knowledge in this area remains limited. Ductile fracture behaviour, influenced by stress states, strain localisation, and microstructural heterogeneities, is a crucial factor in predicting the structural integrity and reliability of WAAM materials. Accurate fracture prediction requires determinations of fracture strain and stress conditions via comprehensive coupon tests and advanced finite element (FE) analysis.

While several studies have examined the mechanical properties of WAAM components—primarily focusing on yield strength and tensile performance of coupons produced using different filler wires [1]-[3]—few have addressed the fracture behaviour in a comprehensive manner.

The prediction of fracture behavior for structural steel have been studied. For instance, [4]proposed a methodology for predicting ductile fracture in high-strength steels using uniaxial stress-strain data, calibrated through FE simulations. This approach was later applied to WAAM-produced steel using ER70-S filler wire [5]. In [6] the influence of Lode angle on fracture initiation was explored and the Lode Angle Modified Void Growth Model was developed, incorporating both stress triaxiality and Lode angle into an exponential fracture strain formulation. Their work also introduced a calibration procedure combining mechanical testing and simulation [7]. Similarly, [8] employed the Gurson-Tvergaard-Needleman (GTN) model to simulate fracture in the heat-affected zone of high-strength steel tubes.

https://doi.org/10.1002/cepa.70052 wileyonlinelibrary.com/journal/cepa

Building on these efforts, the present study aims to systematically investigate the ductile fracture behaviour of WAAM-fabricated materials using a wire composition equivalent to S690 steel. The research combines experimental testing under varying triaxial stress conditions with microstructural analysis to capture different fracture modes. Complementary finite element simulations are used to validate the experimental observations and provide deeper insight into the failure mechanisms unique to WAAM-fabricated structures.

2 Materials and methods

2.1 Materials

In this study the samples were fabricated with high strength low alloy carbon steel utilizing the welding wire *3Dprint AM70* [9] from Voestalpine Böhler with a 1.2 mm diameter. This welding consumable is a solid wire classified as ER100S-G (AWS A5.18) with the chemical composition in Table 1. Based on the selected wire the shielding gas M21 [10] with a mixture of 82% Argon and 18% CO_2 was chosen.

Table 1 Chemical composition of the welding wire and substrate material (wt.%)

C	Mn	Si	Cr	Mo	Ni	Fe
0.08	1.7	0.6	0.2	0.5	1.5	Balance

2.2 Samples manufacturing

The walls with dimensions 310 x 170 mm were produced by depositing single weld beads on matching steel substrate (S690).

The samples were manufactured using Gas Metal Arc Welding (GMAW) in Pulsed mode with 80 A, the robot speed was 5mm/s.

The plates were milled to remove the surface roughness and coupons with dimensions as shown in Figure 1 were cut out of the plates. For each configuration three samples were extracted along the printed direction. The coupons were milled with 4mm thickness.

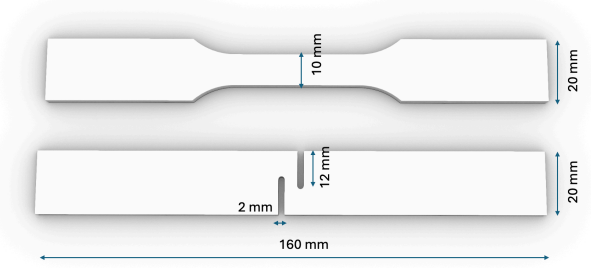

Figure 1 Samples with dimensions

2.3 Experimental setup

The specimens were tested in universal machine with maximum capacity 250 kN, as shown in Figure 2. For measurement of the strains 2D Digital Image Correlation system with Canon EOS5DSR camera was employed taking 2 photos/s using the base length of 30mm.

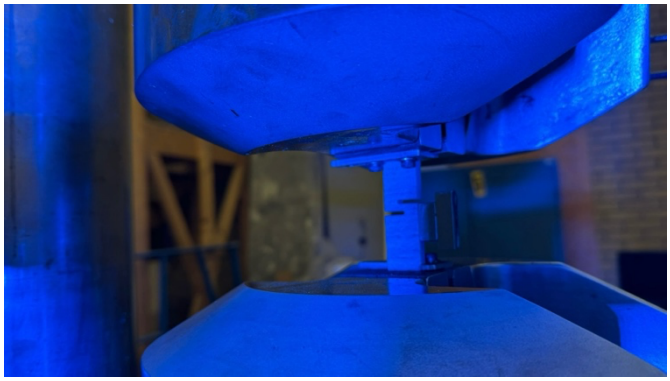

Figure 2 Experimental set-up

2.4 Numerical model

The numerical model was created using Abaqus/CAE 2023 [11]. The samples were modelled with 8-node solid elements with reduced integration C3D8R. The mesh size was constant with the element size 0.5 mm in all directions. To reduce computational effort only the gauge section was modelled.

The results were extracted from points with 30mm the base length cantered in relation to the fracture location, see Figure 3.

For the damage evolution ductile damage with linear law was adopted in the numerical model. The element deletion was set to 0.98. The analyses were run with ABAQUS/Standard and ABAQUS/Explicit.

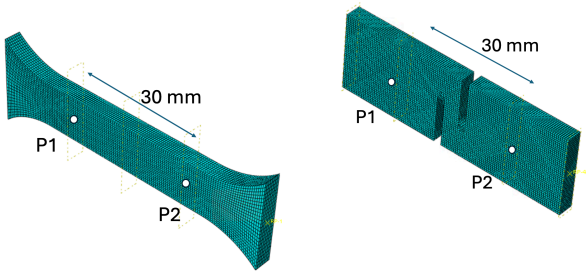

Figure 3 Numerical model and the base length for the deformation

3 Results and discussion

3.1 Experimental results

Representative curves from the uniaxial tension and shear test are shown in Figure 4 and 5 for uniaxial tension and shear, respectively.

The yield and maximum stresses as well as the strains at ultimate stress and at the end of the experiment are presented in Table 2.

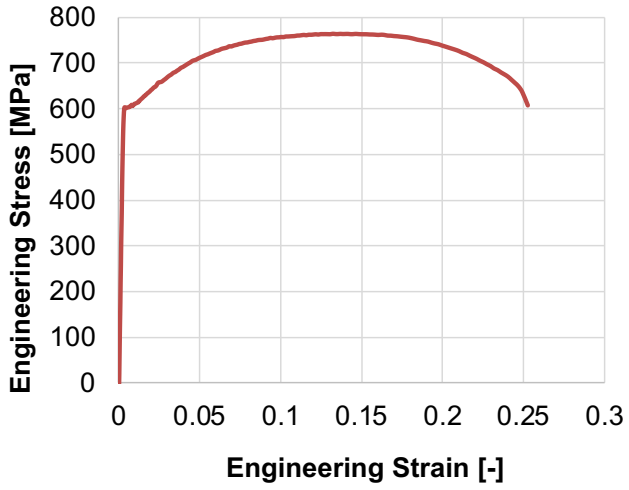

Figure 4 Engineering stress-strain curve for uniaxial tension

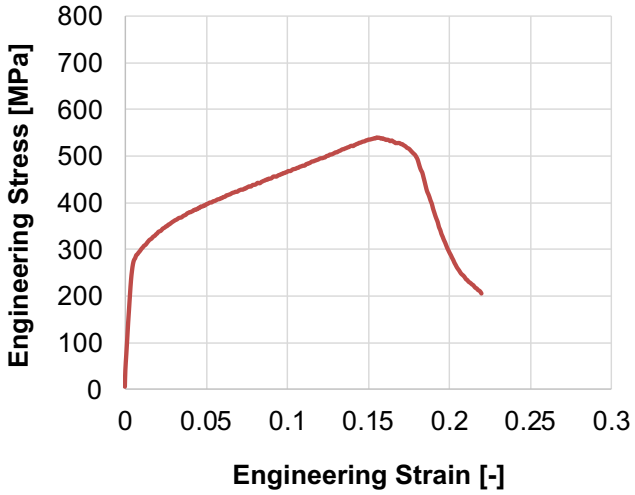

Figure 5 Engineering stress-strain curve for shear coupon

The results show ductile behaviour with slightly lower yield stress than the data sheet for this wire due to size of the wall which leads to higher cooling time.

Table 2 Chemical composition of the welding wire and substrate material (wt.%)

Sample	σ_{yield}	σ_u	ε_u	ε_{max}
T	604 MPa	763 MPa	0.146	0.252
S	289 MPa	540 MPa	0.0067	0.155

3.2 Plasticity parameter identification

To accurately capture the material's plastic behaviour in finite element simulations, the experimental stress-strain response is typically divided into three key regions: (i) the uniform plastic deformation region (pre-necking), (ii) the post-necking region, and (iii) the damage-dominated region leading up to fracture, see Figure 6 (4,5).

In the first region, plasticity dominates, and the material undergoes homogeneous deformation. The engineering stress-strain data obtained from uniaxial tensile tests is converted to true stress σ_{true} and plastic strain ε_p (Eqs 1 and 2) as shown in Figure 6.

$$\sigma_{true} = \sigma_{eng}(1 + \varepsilon_{eng}) \qquad (1)$$

$$\varepsilon_{true} = ln(1 + \varepsilon_{eng}) \qquad (2)$$

This region, extending up to the onset of necking, is crucial for calibrating the initial hardening behaviour of the material.

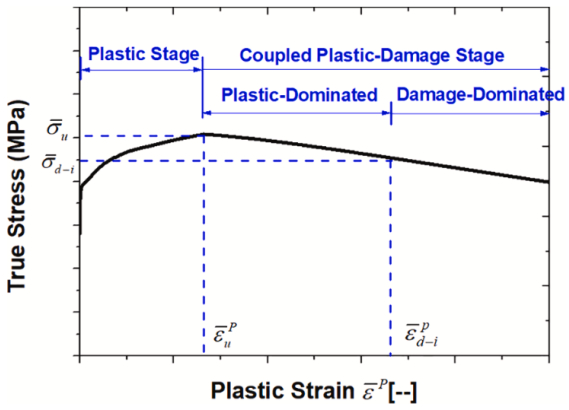

Figure 6 Material behaviour evolution [4]

Once necking begins, the stress and strain states become non-uniform, and direct interpretation of the stress-strain curve becomes invalid. Therefore, in the post-necking region, inverse calibration methods are often employed. This typically involves finite element simulation of the tensile test, where the material model is iteratively adjusted until the simulated force-displacement curve matches the experimental one. In this case, weighted average model was adopted [12] using equation (3):

$$\sigma_{neck} = \sigma_u \left[W(\varepsilon_p - \varepsilon_{p,u}) + (1 - W)\left(\frac{\varepsilon_p}{\varepsilon_{p,u}}\right)^{\varepsilon_{p,u}} \right] \qquad (3)$$

The weight parameter W is calibrated to match the engineering stress-strain curve, where the corresponding plastic strain at the end of plastic region is 0.1331.

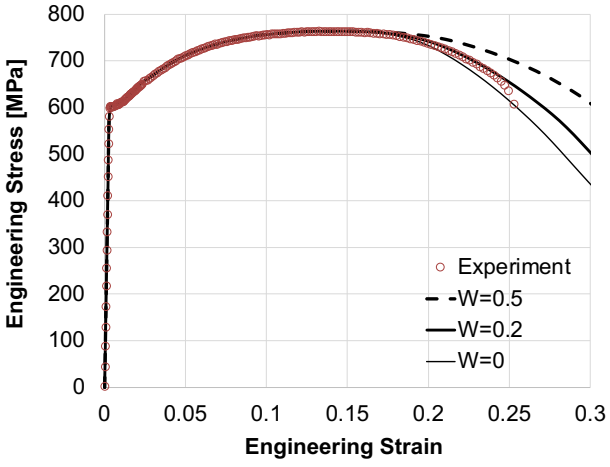

Figure 7 Calibration of weight parameter W for uniaxial tension, no damage considered

An example of different applications is shown in Figure 7. For this the value of W=0.2 was found to be the best match for the experimental results.

Finally, in the damage-dominated region, plastic deformation interacts with void nucleation, growth, and coalescence, marking the transition to fracture. In this study, the damage dominated region calibration was performed using the numerical model and the ductile damage model in Abaqus/CAE.

The final calibrated curves are shown in Figures 8 and 9 for the uniaxial tension and shear respectively. The were computed using Ductile/Shear Damage formulation in Abaqus/CAE. The damage parameters were obtained based on calibration of the numerical model to the experimental curve.

The calibrated parameters are presented in Table 3.

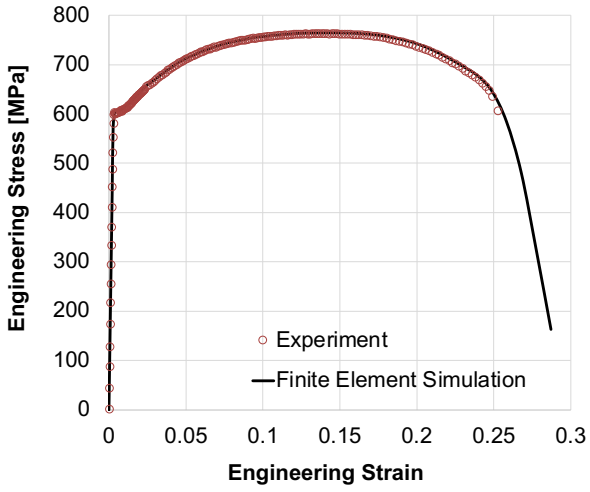

Figure 8 Experimental and numerical engineering curves for uniaxial tension

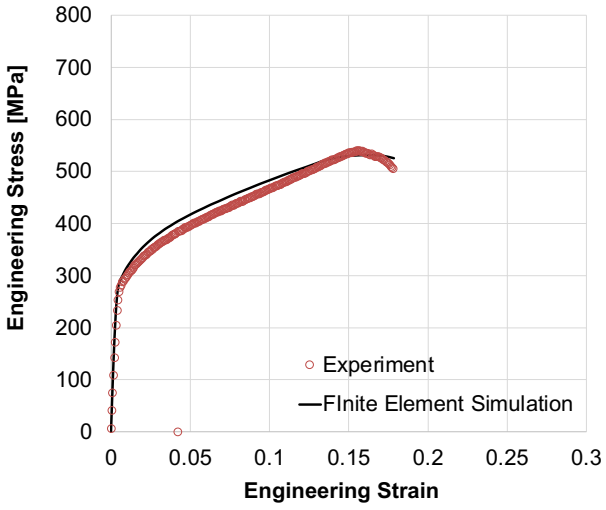

Figure 9 Experimental and numerical engineering curves for uniaxial tension

Table 3 Calibrated fracture strains

Sample	ε_f
Uniaxial tension	0.65
Shear	0.72

Furthermore, the failure mechanisms observed experimentally were compared with those predicted by the finite element simulations. In both cases, a realistic representation of the failure mode was achieved, thereby confirming the reliability and accuracy of the simulation approach in capturing the material's fracture behaviour.

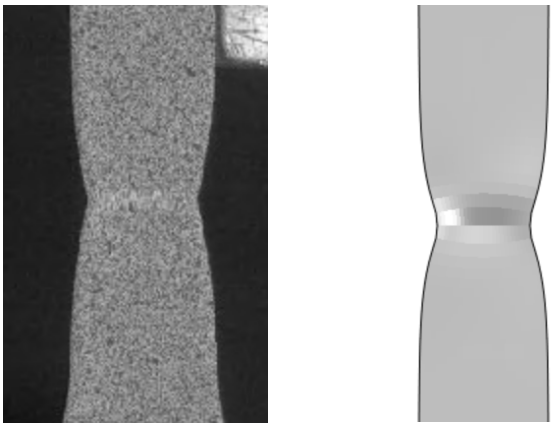

Figure 10 Experimental vs numerical failure mode for uniaxial tension

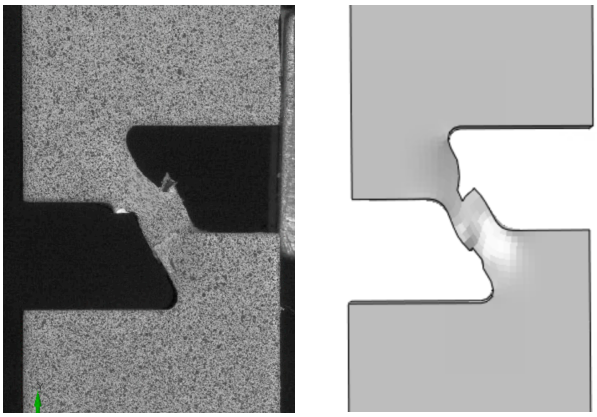

Figure 11 Experimental vs numerical failure mode for shear

3.3 Discussion

In this study, a fracture strain value of 0.65 was determined for the AM70 WAAM-fabricated material. When compared to previously reported envelope fracture strains for WAAM materials with a yield strength of 420 MPa—ranging from 1.1 to 1.5 under uniaxial tension [5] —the current results suggest a somewhat lower ductility. However, when contrasted with high-strength steel (HSS) materials, which exhibited uniaxial tensile fracture strains of 0.237 and 0.264 [4], the AM70 material demonstrates significantly improved performance.

In shear loading conditions, HSS materials showed fracture strains between 0.414 and 0.459, while the WAAM material with 420 MPa yield stress ranged from 0.422 to 0.566. Notably, the AM70 material tested in this study

achieved a shear fracture strain of 0.72, indicating a comparatively higher capacity for deformation under shear.

Although the uniaxial tensile performance of AM70 also exceeds that of HSS, it does so at the expense of slightly reduced yield strength, likely due to slower cooling rate such as material overheating during the deposition process. These findings suggest that AM70 WAAM materials could be particularly advantageous in structural applications subjected to complex loading conditions, where enhanced ductility and energy absorption are essential.

4 Conclusion

This study presents a comprehensive investigation into the ductile fracture behaviour of WAAM-fabricated components produced with AM70 high-strength steel wire. Through a combination of experimental testing under varying stress states and finite element simulations, the mechanical response and fracture characteristics of the material were accurately captured and validated. The calibrated plasticity and damage parameters enabled realistic simulation of both the stress-strain response and failure mechanisms in uniaxial tension and shear conditions.

The AM70 material exhibited a fracture strain of 0.65 in uniaxial tension and 0.72 in shear, indicating a high capacity for plastic deformation—particularly under shear loading. When compared to high-strength steels and previously reported WAAM materials, the AM70 wire demonstrated favourable ductility characteristics, especially in shear, despite a moderate reduction in yield strength likely caused by thermal effects during deposition. These results underscore the potential of AM70 WAAM components for applications requiring enhanced ductility and structural resilience under multiaxial loading.

The methodology employed—combining digital image correlation, experimental calibration, and finite element modelling—provides a robust framework for characterising and predicting fracture behaviour in WAAM structures. As a next step, the integration of established ductile fracture models, such as the Gurson-Tvergaard-Needleman or Lode-angle-based criteria, may offer more accurate and generalisable predictions of failure across a wider range of loading conditions.

References

[1] Tankova, T., Andrade, D., Branco, R., Zhu, C., Rodrigues, D., & Simões da Silva, L. (2022). *Characterization of robotized CMT-WAAM carbon steel*. Journal of Constructional Steel Research, 199,107624.

[2] Huang C, Kyvelou P, Zhang R, Britton T B, Gardner L, (2022). *Mechanical testing and microstructural analysis of wire arc additively manufactured steels*. Materials & Design, 216, 110544.

[3] Müller J, Goulas C, Hensel J, (2024). *Analysis of thermal cycles during DED-Arc of high-strength low-alloy steel and microstructural evolution*. Journal of Materials Research and Technology.

[4] Haohui Xin, Milan Veljkovic, (2021). *Evaluation of high strength steels fracture based on uniaxial stress-strain curves*. Engineering Failure Analysis, 120, 105025.

[5] Haohui Xin, Junqiang Li, Youyou Zhang, Milan Veljkovic, Nicolas Persem, Laurent Lorich, (2025). *Ductile fracture assessment of wire and arc additive manufactured steel materials*. Journal of Constructional Steel Research, 228, 109422.

[6] Xiaofan Liu, Shen Yan, Kim J.R. Rasmussen, Gregory G. Deierlein, (2022). *Experimental investigation of the effect of Lode angle on fracture initiation of steels*. Engineering Fracture Mechanics, 271, 108637.

[7] Jingsheng Zhou, Shen Yan, Kim J.R. Rasmussen, Mengyao Zhang, (2025). *Test-and-FE-based method for obtaining complete stress-strain curves of structural steels including fracture*. Journal of Constructional Steel Research, 224, 109095.

[8] Yan R, Xin H, Mela K, El Bamby H, Veljkovic M. (2022). *Fracture simulation of welded RHS X-joints using GTN damage model*. Advances in Structural Engineering, 26, 2140-2159.

[9] https://www.voestalpine.com/welding/global-en/products/consumables/welding-consumables/wire-arc-additive-manufacturing/, accessed: 7 April 2025

[10] ISO 14175:2008 - Welding consumables — Gases and gas mixtures for fusion welding and allied processes.

[11] Dassault Systèmes. (2023). *Abaqus 2023 User's Manual*. Providence, RI: Dassault Systèmes Simulia Corp.

[12] Y. Ling, *Uniaxial true stress-strain after necking*. AMP J. Technol. 5 (1996) 37–48.